ATLAS NOTE

ATLAS-CONF-2010-089

August 23, 2010

Search for high-mass states with electron plus missing transverse energy using the ATLAS Detector at $\sqrt{s} = 7$ TeV

The ATLAS collaboration

Abstract

The ATLAS detector has been used to search for high-mass states, such as new heavy charged gauge bosons, decaying to an electron plus missing energy. Based on pp collisions at a center of mass energy of 7 TeV produced at the Large Hadron Collider, we present limits on the cross section times branching ratio of $W' \to e\nu$, using the *Sequential Standard Model* (SSM) W' as a benchmark model. With a total integrated luminosity of 317 nb^{-1} we exclude W' particles with masses below 465 GeV at 95% CL.

ATLAS-CONF-2010-089
11 October 2010

1 Introduction

Although the Standard Model of the strong and electroweak interactions is remarkably consistent with particle physics observations to date, the high energy collisions attained by the CERN LHC provide new opportunities to search for extensions to that framework. One extension common to many models is the existence of additional, heavy gauge bosons [1]. It is common to use W' to denote any charge ± 1, spin 1 particle outside the Standard Model and here we adopt that convention and report on the search for a W' boson decaying to an electron and a neutrino whose production is inferred from missing transverse[1] energy.

Measurements at the Fermilab Tevatron experiments [2, 3] rule out the existence of a W' with mass less than 1 TeV assuming the same couplings as those for the Standard Model W boson. Although ATLAS has not yet recorded enough luminosity to improve on this value, we report the limits on σB (the product of the production cross section and the branching fraction) in the electron decay channel over the mass range between 150 and 600 GeV. These limits are based on center of mass energy $\sqrt{s} = 7$ TeV proton-proton collision data with an integrated luminosity of 317 nb^{-1} acquired with the ATLAS detector [4] at the CERN LHC.

We identify candidates for W or W' decay in the electron channel and evaluate the W' mass limit. The kinematic variable used to identify the W' is the transverse mass

$$m_{\mathrm{T}} = \sqrt{2 p_{\mathrm{T}} E_{\mathrm{T}}^{\mathrm{miss}} (1 - \cos\varphi)} \tag{1}$$

which has a Jacobian peak which falls sharply above the boson mass. Here p_T is the electron transverse momentum, $E_{\mathrm{T}}^{\mathrm{miss}}$ is the missing transverse energy (neutrino transverse energy), and φ is the angle between the transverse components of the electron momentum and the missing momentum.

The main background to the W' signal comes from the Standard Model W boson. Other backgrounds are Z bosons decaying into two electrons where one electron is not reconstructed, W or Z decaying to tau leptons where the tau subsequently decays to an electron, and QCD and $t\bar{t}$ production where a light or heavy hadron decays into an electron or a jet is misidentified as an electron.

2 Monte Carlo samples

Monte Carlo simulation samples were produced for a variety of W' masses as well as many Standard Model background processes. With the exception of $t\bar{t}$, all samples were generated with Pythia 6.421[5] using MRST LO* [6] parton distribution functions (PDF). For all samples, the propagation of particles and the response of the detector were evaluated using ATLAS full detector simulation [7] based on Geant4 [8]. Reference [9] describes how the parameters in the above generators were tuned to match measurements from the Tevatron.

The Pythia signal model used as a benchmark for W' is the *Sequential Standard Model* (SSM). In this model, the new heavy gauge bosons have the same couplings as their Standard Model counterparts. Table 1 lists the W' signal samples that were simulated and the cross sections obtained in the event generation.

Table 2 lists the Monte Carlo background samples and their cross sections. The $W \to e\nu$ and $Z \to ee$ cross sections were calculated at next-to-next-to-leading order (NNLO) using FEWZ [10] with MSTW2008 parton distribution functions [11]. Samples denoted $W \to l\nu(m_1, m_2)$ include all leptonic decays (e, μ and τ) and are generated over the restricted mass range $m_1 < m_W < m_2$. The cross sections for these are obtained by scaling the NNLO total cross section by the ratio of the generated Pythia cross sections with and without the mass restriction. Events in the unrestricted W samples are excluded if their mass falls in the range covered by the restricted samples.

[1] Throughout this note, the longitudinal direction is parallel to the colliding beams and the transverse plane is perpendicular.

Mass [GeV]	Γ(GeV)	B	σB [pb]	N_{evt} [k]
150	3.88	0.1084	1296	60
200	5.34	0.1054	495	60
300	9.18	0.0924	109	60
400	12.98	0.0874	36.8	60
500	16.68	0.0852	15.5	60
600	20.34	0.0840	7.6	54

Table 1: Monte Carlo signal samples. The first column is the W' mass and the second is the width. The third and fourth are the branching fraction and cross section times branching fraction for $W' \to e\nu$. The last column is the number of generated events. The cross section, width and branching fraction are calculated with PYTHIA for the SSM.

Category	Process	σB [nb]	N_{evt} [k]
W/Z	$W \to e\nu$	10.45	7000
	$W \to \tau\nu \to \ell\nu\nu$	3.68	1000
	$W \to l\nu$(200,500)	0.01041	60
	$W \to l\nu$(500,1500)	0.000283	60
	$Z \to ee$	0.989	5300
$t\bar{t}$	$t\bar{t} \to lX$	0.161	1000
QCD	$jj(8, 17)$	9860000	1400
	$jj(17, 35)$	673000	1400
	$jj(35, 70)$	41200	1400
	$jj(70, 140)$	2190	1400
	$jj(140, 280)$	87.9	1400
	$jj(280, 560)$	2.33	1400
	$jj(560, 1120)$	0.339	1400

Table 2: Monte Carlo samples used to estimate backgrounds. The first two columns are the category and physics process, next is the cross section times branching fraction, and last is the number of generated events (in thousands).

The $t\bar{t}$ background was generated with MC@NLO 3.41 [12] to generate matrix elements, JIMMY 4.31 to describe multiple parton interactions [13] and HERWIG 6.510 [14, 15] to describe the remaining underlying event and parton showers. CTEQ6.6 [16] parton distribution functions were used. The $t\bar{t}$ cross section is calculated at near-NNLO using the results from reference [17] and assuming a top mass of 172.5 GeV.

The remaining QCD background is simulated using PYTHIA hard-QCD processes, i.e. quark-quark, quark-gluon and gluon-gluon scatters denoted by $jj(p_1, p_2)$ for inclusive production. The arguments indicate the allowed range of the transverse momentum of the hard scatter: $p_1 < p_{\text{T}} < p_2$. The tabulated cross section is that calculated with PYTHIA but, for the following plots and limit calculations, the QCD background rate is scaled (see section 7) to the data in the QCD-dominated transverse-mass region below the W boson Jacobian peak.

3 ATLAS detector, trigger and event reconstruction

The ATLAS detector [4] has several major components. Tracks and vertices are reconstructed with silicon pixel, silicon strip and transition radiation detectors covering $|\eta| < 2.5$ and immersed in a homogeneous 2 Tesla magnetic field provided by a superconducting solenoid. These are surrounded by a finely-segmented, hermetic calorimeter that covers $|\eta| < 4.9$ and provides three-dimensional reconstruction of particle showers using liquid argon for the inner electromagnetic compartment followed by a hadronic compartment based on scintillating tiles in the central region and additional liquid argon for $|\eta| > 1.8$. Outside the calorimeter, there is a muon spectrometer with three air-core toroids providing a non-uniform magnetic field integral averaging about 3 Tesla-m. Drift tubes and cathode strip chambers provide precision measurements and resistive-plate and thin-gap chambers provide triggering capability and measurement of the non-precision (φ) coordinate.

A hardware-based (first level) trigger is used to select proton-proton collisions of interest, and software algorithms are applied to these candidates in a two-stage high-level trigger that determines which events are recorded for offline processing. The data used for this study required the presence of a 10 GeV electron in the first-level trigger with no additional selection criteria imposed at the higher levels. All accepted events were processed to reconstruct tracks in the inner detector and muon spectrometer, find vertices (including the primary interaction vertex) from the inner detector tracks, and reconstruct physics objects such as electrons, muons and jets.

Energy clusters are reconstructed in the electromagnetic compartment with a sliding window algorithm and then identified as electrons using their transverse shape and longitudinal leakage into the hadronic compartment, and by matching with an inner detector track. The electron energy is obtained from the cluster and its direction from the track. ATLAS defines three levels of electron identification: loose, medium and tight [18]. This study makes use of the second of these for which shower-shape and track-matching criteria give about 95% identification efficiency for electrons with $p_{\mathrm{T}} > 200$ GeV and a rate of 1/5000 to falsely identify jets as electrons before isolation requirements are imposed [18].

The neutrino is not detected directly but the transverse components of its momentum are taken to be the missing E_{T}, i.e. the transverse energy required to balance the other objects reconstructed in the event. The missing E_{T} is obtained from a vector sum over calorimeter cells associated with topological clusters [18]:

$$\mathbf{E}^{\mathrm{miss}}_{\mathrm{Tcalo}} = -\sum \mathbf{E}_T \tag{2}$$

Use of this sum rather than summing over all cells reduces the noise contribution and improves the precision of the measurement. The resolution of this $E^{\mathrm{miss}}_{\mathrm{T}}$ measurement is $0.41\sqrt{\sum E_{\mathrm{T}}}$ where the scalar transverse energy sum also includes only cells associated with topological clusters. Topological clusters are first classified either as hadronic or electromagnetic according to the cluster topology. Each cluster is assigned a weight according to the cluster and cell energy density. A further correction is added to account for inactive material. These weights are determined from charged and neutral pion Monte Carlo simulations and applied to all calorimeter cells. Details may be found in reference [19].

4 Event selection

Events are recorded and luminosity is measured in blocks of time typically lasting about two minutes and the detector status and data quality are evaluated for each such block. Data from a block are not considered for this analysis if problems are found in the inner detector, calorimeter, trigger, or in the measurement of the beam position or luminosity. The integrated luminosity for the data used in this study is 317 nb^{-1}, with an uncertainty of 11% [20].

Events are required to have a primary vertex reconstructed from at least three tracks with p_{T} above 150 MeV and longitudinal distance less than 15 cm from the center of the collision region. Spurious tails

in $E_{\mathrm{T}}^{\mathrm{miss}}$ arising from calorimeter noise are suppressed by checking the quality of each reconstructed jet and discarding events with any jet which has a shape indicating possible noise contamination following standard ATLAS criteria for *jet cleaning* [21].

Events are required to have a candidate electron defined as follows. A candidate electron is one reconstructed with $E_T > 20$ GeV, $|\eta| < 1.37$ or $1.52 < |\eta| < 2.47$ and satisfying the ATLAS medium electron requirement described above. In addition, a fiducial cut is made to remove events with electrons near problematic regions of the electromagnetic calorimeter. This removes about 5% of the acceptance. In addition, the inner detector track associated with the electron is required to be close to the primary vertex, specifically with transverse distance of approach satisfying $|r_0^{\mathrm{PV}}| < 1$ mm and longitudinal distance at this point $|z_0^{\mathrm{PV}}| < 5$ mm. Events are required to have exactly one candidate electron.

Figure 1 shows the inclusive transverse mass (m_{T}) distributions obtained after initial event selection (events satisfying the criteria defined above) for ATLAS data, for the expected background and for a few examples of W' signal at different masses on top of the background. With the current integrated luminosity, there is clear observation of the Standard Model W boson.

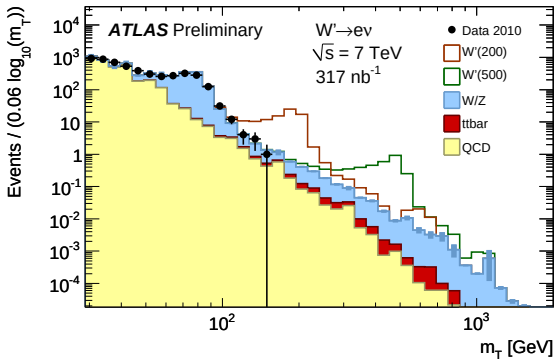

Figure 1: Transverse mass spectra after initial selection. Points are ATLAS data and the filled histograms show the Monte Carlo background from QCD, that plus $t\bar{t}$, and that plus W and Z boson contributions. Open histograms are W' signals added to the background. All Monte Carlo is normalized to the data integrated luminosity using the cross sections from Table 2 except the QCD is scaled to data at low m_{T} (see section 7).

The major background is the irreducible tail of the Standard Model W boson but there are also contributions from $t\bar{t}$ and other QCD sources. To suppress the latter, we require the electron to be isolated, defining isolation by

$$R_{\mathrm{isol}} = \frac{\sum p_{\mathrm{T}}^{\mathrm{trk}}}{p_{\mathrm{T}}^{\mathrm{e}}} \tag{3}$$

and requiring $R_{\mathrm{isol}} < 0.05$. Here $p_{\mathrm{T}}^{\mathrm{e}}$ is the electron transverse momentum and the sum in the numerator is over the transverse momenta of the inner detector tracks with $p_{\mathrm{T}}^{\mathrm{trk}} > 1.0$ GeV in a cone $\Delta R < 0.30$ ($\Delta R = \sqrt{(\Delta\eta)^2 + (\Delta\varphi)^2}$) around the direction of the electron. Figure 2 shows the observed isolation distributions and their Monte Carlo predictions after initial selection, and the missing E_{T} distribution obtained after imposing, in addition, the isolation requirement. For the final selection, we additionally require $E_{\mathrm{T}}^{\mathrm{miss}} > 25$ GeV and the final p_{T} and m_{T} spectra are shown in Figure 3. The agreement between data and Monte Carlo is good at all stages.

The p_{T} and m_{T} spectra show no evidence for the existence of a W' and the data are used to set limits on σB for a series of W' masses ranging from 150 to 600 GeV. Limits are obtained by counting the number of events with $m_{\mathrm{T}} > 0.7 m_{W'}$.

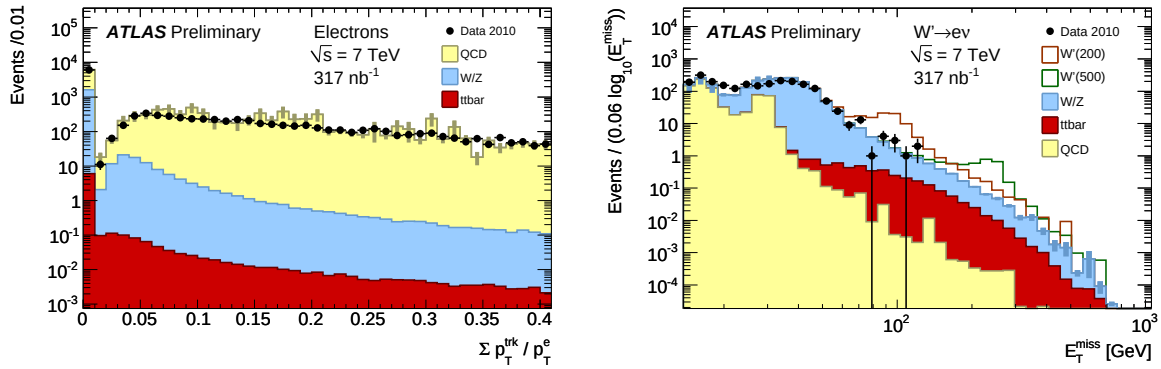

Figure 2: Left: isolation spectra after initial selection. Points are ATLAS data and the filled histograms show the Monte Carlo background from $t\bar{t}$, that plus W and Z contributions, and that plus QCD. Right: missing E_{T} spectra after initial selection and isolation. The Monte Carlo normalization is the same as that in Figure 1.

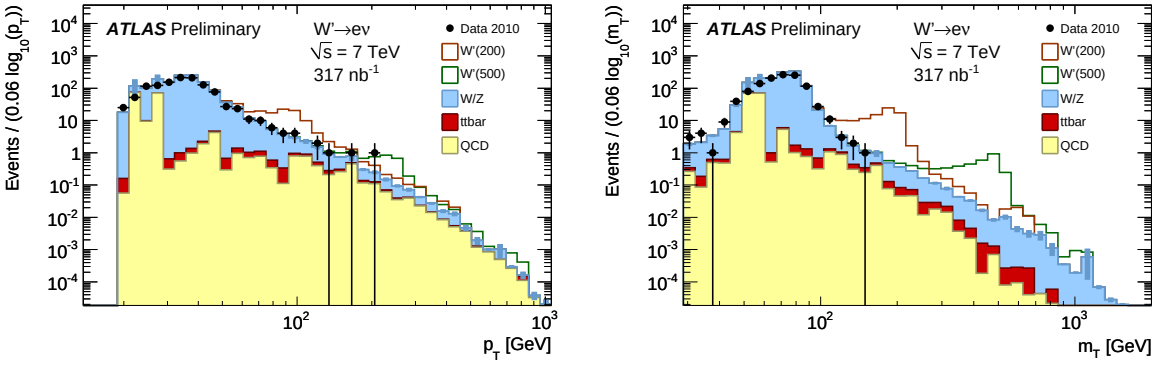

Figure 3: Transverse momentum (left) and transverse mass (right) spectra after the final selection. Points and histograms have the same meaning as in Figure 1.

Table 3 gives the number of events passing each stage of selection for the data and for each Monte Carlo category.

5 Likelihood function

A single-bin likelihood analysis is performed to set a limit at each mass using the observed number of events with $m_{\mathrm{T}} > 0.7 m_{W'}$. The expected number of events is

$$N = \varepsilon L_{\mathrm{int}} \sigma B + N_{\mathrm{bg}} \tag{4}$$

where L_{int} is the integrated luminosity of the data sample and ε is the event selection efficiency, i.e. the fraction of events that fall within detector acceptance, pass all event selection criteria and have m_{T} above threshold. The last term is the expected number of background events and is obtained from Monte Carlo using the same selection criteria:

$$N_{\mathrm{bg}} = \sum s_i (\varepsilon\sigma)_i L_{\mathrm{int}} \tag{5}$$

where the sum is over all relevant background processes labeled with index i. Here $(\varepsilon\sigma)_i$ is the Monte Carlo cross section to pass all selection criteria and have m_{T} above threshold and s_i is a scale factor to

Process	Initial	Isolation	Final	$m_T > 140$	$m_T > 350$
Collision Data	12242	6615	1180	1	0
W'(200)	105	103	101	75	
W'(500)	3.8	3.75	3.74		2.5
W/Z	1709	1656	1250	3.71	0.11
$t\bar{t}$	7.0	6.5	5.5	0.45	0.0093
QCD	12929	5277	178	1.18	0.007

Table 3: Selected event counts for the collision data and the Monte Carlo samples for both signal and background. The first column is the data source while the following are the selected event counts scaled to the integrated luminosity of the collision data. The first count is the initial selection, followed by that plus isolation and that plus the E_T^{miss} cut (final selection). The last three columns give the number of selected events after the indicated m_T threshold is applied, i.e. for W' masses of 200 and 500 GeV. Monte Carlo counts are scaled to the integrated luminosity of the data of 317 nb^{-1} using the cross sections from Tables 1 and 2 except QCD is scaled to fit the data at low m_T (section 7).

correct the Monte Carlo. The integrated luminosity L_{int} is again that for the data, i.e. that which appears in equation 4.

Using Poisson statistics, we obtain the likelihood to observe N_{obs} events:

$$\mathcal{L}(\sigma B) = \frac{(L_{int}\varepsilon\sigma B + N_{bg})^{N_{obs}} e^{-(L_{int}\varepsilon\sigma B + N_{bg})}}{N_{obs}!} \tag{6}$$

and this expression is used to set limits on σB. Uncertainty in any of the parameters characterizing this expression are included by multiplying by the pdf (probability density function) characterizing that uncertainty. In general, if N such nuisance parameters $\theta_1, ..., \theta_N$ are identified, then the likelihood becomes

$$\mathcal{L}(\sigma B, \theta_1, ..., \theta_N) = \frac{(L_{int}\varepsilon\sigma B + N_{bg})^{N_{obs}} e^{-(L_{int}\varepsilon\sigma B + N_{bg})}}{N_{obs}!} \prod g_i(\theta_i) \tag{7}$$

where $g_i(\theta_i)$ is the pdf for parameter θ_i. For example, we model the integrated luminosity using a Gaussian pdf with mean $\bar{L}_{int}$ and RMS σ_{Lint}, i.e.

$$g_{Lint}(L_{int}) = \frac{1}{\sqrt{2\pi}\sigma_{Lint}} e^{-\frac{(L_{int}-\bar{L}_{int})^2}{2\sigma^2_{Lint}}} \tag{8}$$

The value used for σ_{Lint} is the 11% uncertainty on the integrated luminosity. Uncertainties on the selection efficiency and number of background events are handled in the same way: each is assigned a value and an uncertainty and then described with a Gaussian pdf characterized by those parameters; the effect of these uncertainties is then computed by integrating $\mathcal{L}(\sigma B, \theta_1, ..., \theta_N)$ over the phase space of the various nuisance parameters $\theta_1, ..., \theta_N$. The main uncertainties considered in this analysis are described in the next two sections.

6 Event selection efficiency and systematic uncertainties

The Monte Carlo samples are used to extract initial estimates for the event selection efficiencies, ε_{MC}, by counting the fraction of events that pass all selection cuts and have transverse mass above threshold. The final estimate for the selection efficiency is evaluated by applying a correction factor to account for biases in the Monte Carlo.

6.1 Electron Trigger

The electron trigger efficiency has been measured in minimum bias collision data (events which pass the electron medium offline selection and a lower threshold trigger are preselected and the relative efficiency of the 10 GeV electron trigger is evaluated on this sample). The trigger efficiency for electrons above E_T=10 GeV was measured to be 99.5% with respect to the offline electron medium identification. This is in good agreement with the simulated electron trigger efficiency, and no further correction is applied.

6.2 Electron reconstruction efficiency and energy scale

Systematic uncertainties related to the electron reconstruction and identification, in particular due to material effects, and to the fiducial cuts have been evaluated as part of a measurement of the $W \to e\nu$ cross section [22]; we follow that study and assign an uncertainty of 8.0% on the total event selection efficiency. Following the procedures used in that study, we find an overall efficiency loss of 7.6% in data with respect to the Monte Carlo expectation for the cuts used in the analysis presented here; accordingly, we assign an efficiency correction factor of 0.924. To study the effect of the uncertainty on the electron energy scale, we varied it by ±3% (as for the measurement of the $W \to e\nu$ cross section [22]) and obtained an additional 2% systematic uncertainty to the event selection efficiency. Test-beam measurements performed up to energies of 250 GeV [23] cover the kinematic range required to explore the sensitivity to W' boson signals with masses up to 500 GeV, using the above systematic uncertainties.

6.3 Missing E_{T} scale and resolution

The energy scale and resolution of the ATLAS missing E_{T} measurement are discussed in references [19] and [22]. Our event selection requires the presence of a single high-p_{T} electron which typically makes the largest contribution to the missing E_{T}. Any systematic correction to or uncertainty arising from the electron contribution to the missing E_{T} is strongly correlated to the correction or uncertainty associated with the measurement of the electron p_{T}. Consequently, the event selection efficiency-corrections and uncertainties associated with the electron part of the missing E_{T} are combined with those arising from the electron, i.e. are implicitly included in the systematic corrections arising from the measurement of the electron energy.

Here we evaluate systematic effects arising from the remaining contribution to $E_{\mathrm{T}}^{\mathrm{miss}}$, e.g. that from the underlying event. The missing E_{T} resolution is fairly well modeled by the Monte Carlo [19] and it is the energy scale of the measurement of low energy depositions which is the dominant systematics effect. The uncertainty on the cluster energy scale of these depositions is derived as the difference between data and Monte Carlo simulation in the context of E/p studies. It varies from 20% to 5% for transverse momenta varying from 0.5 to 50 GeV. To evaluate the effect on the W' measurement, all cluster energies except that of the electron were varied up and down by 20% for each of the W' Monte Carlo signal samples and the largest change in the efficiency was 0.6%. We assign this value, σ_{MET} = 0.6%, as the systematic uncertainty on the event selection efficiency arising from the non-electron part of the missing E_{T} measurement.

7 Background event counts

Backgrounds are estimated using the Monte Carlo simulation with the total background for each mass and decay channel calculated according to equation 5 which includes a scale factor for each background contribution. The uncertainty on the number of background events depends on the uncertainty on the scale factor and, for the W/Z and $t\bar{t}$ backgrounds, also on the uncertainty on the estimated cross sections. We estimate the uncertainty for the dominant $W \to e\nu$ background and use the same value for the other

background contributions. Three sources are considered to evaluate the uncertainty on the $W \to e\nu$ cross section: mass dependence, scale variation and PDF (parton density function) uncertainties. The next-to-leading (NLO) order generator MCFM [24] was used to study the mass dependence of the PYTHIA differential cross section. The fraction of the sample in bins at high mass is slightly lower in PYTHIA: 3% lower in the bin $0.7 < m_W < 1.0$ TeV. The scale factors in the MCFM calculation were varied up and down by a factor of two and the change was less than 2% for these bins and lower masses. We did not estimate PDF errors directly for the W/Z samples but did study the effect of varying the PDF eigenvectors in PYTHIA calculations of W' cross sections which are expected to have the same PDF dependence as the W. Following the prescription in [18] (i.e. adding eigenvector variations in quadrature), we found variations of 4-6% from the central value for $0.1 < m_{W'} < 1.0$ TeV using MSTW200 [11] PDF's. Based on these results for mass dependence, scale variation and varying PDF eigenvectors, we assign a systematic uncertainty of 7% to the $W \to e\nu$ cross sections used to estimate our backgrounds.

For the QCD background (which constitutes less than 10% of the total background for $m_{W'}$ above 400GeV), the scale factor was chosen to make the Monte Carlo agree with the data after the isolation cut for $20 < m_{\mathrm{T}} < 40$ GeV, where QCD is the dominant contribution. The QCD scale factor is 0.455. Different definitions of this scale factor (using different m_{T} regions, or based on isolation variables) produce results within 20% of this value, but an uncertainty of 40% is used in the limit calculations to account for uncertainty in the extrapolation to high m_{T}.

No attempt was made to fit the data for the other backgrounds (W/Z and $t\bar{t}$). Instead the estimates are taken from the Monte Carlo simulation using the cross sections from table 2 along with the scale factor used for the W' signal.

8 Summary of systematic uncertainties

Table 4 shows the systematic uncertainties used for the calculation of the limits. Besides the luminosity uncertainty, the main uncertainties are those coming from electron identification, material effects and fiducial cuts. The effect of the large QCD scale factor uncertainty decreases as the m_{T} cut value increases. The impact of event pileup is negligible with respect to the other uncertainties considered.

Source	Size [%]
Event selection	
Identification, material, fiducial cuts	8.0
Electron energy scale	2.0
Low energy component of $E_{\mathrm{T}}^{\mathrm{miss}}$	0.6
Background	
Mass dependence, scale and PDF variation	7.0
QCD scale factor for $m_{\mathrm{T}} > 300$ GeV	<5.0
Common	
Total integrated luminosity	11.0

Table 4: Summary of systematic uncertainties.

9 Limits

Limits for 95% CL exclusion on σB for each W' mass are set using the likelihood function in equation 7 as input to the estimator

$$CL_s = \frac{CL_{s+b}}{CL_b} \tag{9}$$

following reference [25]. Inputs to this calculation include the observed number of events, the signal efficiencies and uncertainties described in the previous section, the integrated luminosity of 317 nb^{-1}, and the number of background events. Table 5 gives the number of observed events and total number of background events for each W' mass and decay channel after applying all selection criteria including the m_{T} threshold. The number of events predicted for an SSM W' boson (Pythia LO cross section) are also shown but are not used in the limit calculation.

W' mass [GeV]	N_{obs}	N_{bg}	N_{pred}
150	14	14.5 ±1.9	175
200	1	5.0 ±0.7	75
300	0	1.03 ±0.12	17.4
400	0	0.29 ±0.03	5.9
500	0	0.107±0.012	2.5
600	0	0.037±0.003	1.2

Table 5: Event counts after final event selection. The first column is the W' mass. The last three are the observed number of events, the expected number of background events (all sources and including scale factors) and the number predicted by Pythia for an SSM W' at NLO. The uncertainty in the background count does not include the contribution from the integrated luminosity.

The systematic uncertainties used in the limit calculations include the uncertainty on the number of background events (Table 5), the event selection efficiency uncertainties, and the uncertainty on the integrated luminosity. These are assumed to be uncorrelated.

Table 6 and Figure 4 show the 95% CL limit for each mass point. In addition to limits with all the systematic corrections and uncertainties, limits neglecting the uncertainty on the integrated luminosity are also presented. The difference with the full systematics case is quite small. Finally, results are shown for "no systematics" where all systematic uncertainties are neglected (i.e. no nuisance parameters). Figure 4 also shows Monte Carlo predictions for the range of expected limits for fluctuations up to one and two standard deviations in background level.

Figure 4 also shows the Pythia LO estimate of the $W' \to e\nu$ SSM cross section times branching fraction for each mass.

The intersection between the limits and these values provides a 95% CL estimate upper limit on the W' mass in the SSM model. Using linear interpolation between the points, we obtain limits of 465 GeV with this integrated luminosity.

10 Conclusions

With approximately 317 nb^{-1} of 7 TeV pp collisions, we see no excess over background and exclude an SSM W' with mass less than 465 GeV at 95% CL. This observation is consistent with the limits observed at the Tevatron (1.0 TeV).

$m_{W'}$	95% CL limit on σB [pb]		
[GeV]	No sys.	No lumi.	Full sys.
150	70.0	74.8	84.0
200	24.5	24.9	26.0
300	20.3	20.6	21.4
400	20.3	20.6	21.3
500	20.0	20.3	20.9
600	20.0	20.2	21.0

Table 6: Limits on W' σB. The first column is the W' mass and the last three are 95% CL limits without systematic uncertainties, limits including all systematic effects except the uncertainty on the integrated luminosity, and limits with all systematic uncertainties.

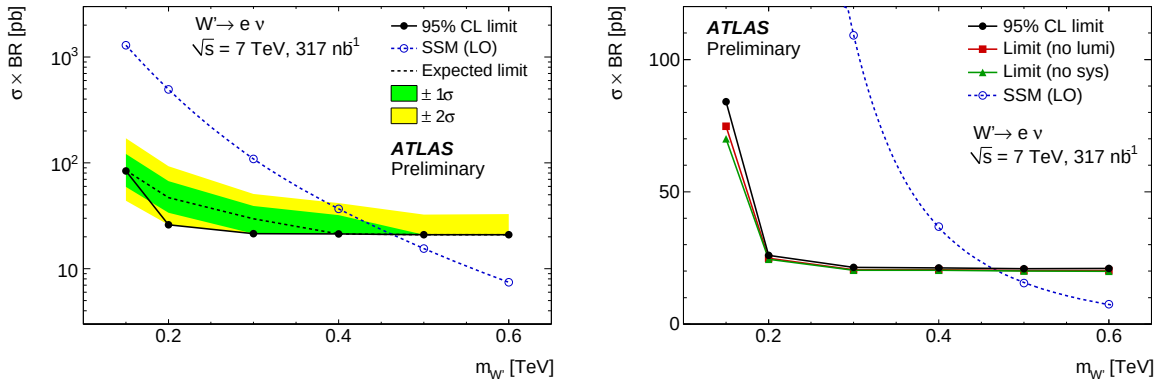

Figure 4: Limits on W' production. Limits and the PYTHIA SSM predictions are shown on both log (left) and linear (right) scales. The latter includes two additional sets of limits: those set without accounting for uncertainty on the integrated luminosity and those without including any systematic uncertainties.

References

[1] C. Amsler, *Review of Particle Physics*, Physics Letters B **667** (2008) .

[2] The D0 Collaboration, A. Abazov et al., *Search for W' Bosons Decaying to an Electron and a Neutrino with the D0 Detector*, Phys. Rev. Lett. **100** (2008) 031804.

[3] The CDF Collaboration, A. Abulencia et al., *Search for W' Bosons decaying to electron-neutrino pairs in $p\bar{p}$ collisions at $\sqrt{s} = 1.96$ TeV*, Phys. Rev. **D75** (2007) 091101.

[4] The ATLAS Collaboration, G. Aad et al., *The ATLAS Experiment at the Large Hadron Collider*, JINST **3** (2008) S08003.

[5] S. M. T. Sjostrand and P. Skands, *PYTHIA 6.4 physics and manual*, JHEP **05** (2006) 026.

[6] A. Sherstnev and R. S. Thorne, *Parton Distributions for LO Generators*, Eur. Phys. J. **C55** (2008) 553.

[7] The ATLAS Collaboration, G. Aad et al., *The ATLAS Simulation Infrastructure*, Eur. J. Phys. C **submitted** (2010) .

[8] The GEANT4 Collaboration, S. Agostinelli et al., *GEANT4: A simulation toolkit*, Nucl. Instrum. Meth. **A506** (2003) 250.

[9] The ATLAS Collaboration, G. Aad et al., *ATLAS Monte Carlo Tunes for MC09*, ATL-PHYS-PUB-2010-002 .

[10] C. Anastasiou, L. Dixon, K. Melnikov, and F. Petriello, *High-precision QCD at hadron colliders: electroweak gauge boson rapidity distributions at NNLO*, Phys. Rev. **D69** (2004) 094008.

[11] A. Martin, W. Stirling, R. Thorne, and G. Watt, *Parton Distributions for the LHC*, Eur. Phys. J. **C63** (2009) 189.

[12] S. Frixione and B. Webber, *Matching NLO QCD computations and parton shower simulations*, JHEP **0206** (2002) 029.

[13] J. M. Butterworth and M. H. Seymour, *Multi-parton interactions in Herwig for the LHC*, http://projects.hepforge.org/jimmy .

[14] G. Corcella, I. Knowles, G. Marchesini, S. Moretti, K. Odagiri, P. Richardson, M. Seymour, and B. Webber, *HERWIG6: an event generator for hadron emission reactions with interfering gluons (including supersymmetric processes)*, JHEP **01** (2001) 010.

[15] G. Corcella, I. Knowles, G. Marchesini, S. Moretti, K. Odagiri, P. Richardson, M. Seymour, and B. Webber, *HERWIG 6.5 Release Note*, arXiv:hep-ph/0210213 .

[16] P. M. Nadolsky et al., *Implications of CTEQ global analysis for collider observables*, Phys. Rev. **D19** (2010) .

[17] U. Lagenfeld, S. Moch, and P. Uwer, *Measuring the running top-quark mass*, Phys. Rev. **D80** (2009) 054009.

[18] The ATLAS Collaboration, G. Aad et al., *Expected Performance of the ATLAS Experiment: Detector, Trigger and Physics*, CERN-OPEN-2008-020 (2009) .

[19] The ATLAS Collaboration, *Performance of the Missing Transverse Energy Reconstruction and Calibration in Proton-Proton Collisions at a Center-of-Mass Energy of* $\sqrt{s} = 7$ *TeV with the ATLAS Detector*, ATLAS-CONF-2010-057 (2010) .

[20] The ATLAS Collaboration, *Luminosity Determination Using the ATLAS Detector*, ATLAS-CONF-2010-060 (2010) .

[21] The ATLAS Collaboration, G. Aad et al., *Data-Quality Requirements and Event Cleaning for Jets and Missing Transverse Energy Reconstruction with the ATLAS Detector in Proton-Proton Collisions at a Center-of-Mass Energy of* $\sqrt{s} = 7$ *TeV*, PLHC (2010) .

[22] The ATLAS Collaboration, *Measurement of the* $W \to l\nu$ *production cross-section and observation of* $Z \to ll$ *production in proton-proton collisions at* $\sqrt{s} = 7$ TeV *with the ATLAS detector*, ATLAS-CONF-2010-051 (2010) .

[23] M. Aharrouche et al., *Measurement of the response of the ATLAS liquid argon barrel calorimeter to electrons at the 2004 combined test-beam*, Nucl. Instr. Meth. **614** (2010) 400.

[24] J. M. Cambell and R. K. Ellis, *Radiative corrections to* $Zb\bar{b}$ *production*, Phys. Rev. **D62** (2000) 114012.

[25] T. Junk, *Confidence level computation for combining searches with small statistics*, Nucl. Instr. Meth. **434** (1999) 091101.